Voltage Feedback Current Control Scheme for Improved Transient Performance of Permanent Magnet Synchronous Machine Drives

Yong-Cheol Kwon, *Student Member, IEEE*, Sungmin Kim, *Student Member, IEEE*, and Seung-Ki Sul, *Fellow, IEEE*

***Abstract*—This paper proposes a novel control scheme for the fast current control of permanent magnet synchronous machines. The proposed method mainly works in the transient state of current control without deteriorating steady-state characteristics. The proposed method is applicable in a wide range of speed: in the speed below the base speed and in the flux weakening region. Using the proposed method, the reference values of $d-q$ currents are modified so that the currents follow the so-called "shortcut" trajectory in the $d-q$ coordinate plane. The effectiveness of the proposed method is confirmed by computer simulations and experiments. The settling time is reduced by 55% compared with that of the conventional method.**

***Index Terms*—Current regulation, fast transient response, permanent magnet synchronous machine (PMSM).**

I. Introduction

In INDUSTRIAL applications of high-performance ac motor drive systems, permanent magnet synchronous machines (PMSMs) are widely used because of its higher torque density and efficiency. In applications such as traction, robotics, or spindle drives, steady-state current regulation, as well as the fast transient response of the current, is required. Because the current is controlled by the machine terminal voltage provided by an inverter, a well-designed current regulator that produces proper voltage reference is imperatively necessary.

Among the many types of current regulator schemes, the synchronous-frame proportional–integral (PI) current regulator [1] is widely used for high-performance machine drive systems. Because the synchronous current controller regulates the direct and quadrature (d-/q-axis) currents separately from the dc values, its structure is simple and the controller gains can be easily determined. In the voltage unsaturated condition where the outputs from the current regulator are linearly synthesized by the PWM inverter, the currents are well regulated as designed. If abrupt reference changes are applied above medium speed range, the voltages from the current regulator easily go beyond the limits of the dc-link voltage and the outputs of the current regulator are saturated. In a saturated condition, because the voltage references cannot be linearly synthesized, the degradation of current regulation is inevitable.

There have been many approaches to achieving a fast current control response in the case of the saturation of the current regulator. One approach is selecting a proper voltage vector on the hexagonal voltage boundary by devising an overmodulation method [2]–[6]. In [3] and [4], the output voltages of the current controller are divided into two components: One is in phase with the effective back-EMF, and the other is in phase with the dynamic voltage, which invokes current variation. To minimize the current distortion in the transient state, only the dynamic voltage is modified while keeping the effective back-EMF. Lerdudomsak *et al.* in [5] and [6] focused on the torque variation during transient time and selected a voltage vector for the fast torque response. However, because overmodulation approaches are based only on the outputs of the current regulator itself, they have inevitable limitations in transient performance. To be more specific, q-axis voltage deficiency, which becomes larger in high-speed operation, is not considered in the conventional current control scheme. Because of this, in dynamic operational conditions such as abrupt reference change, the current regulator does not produce proper voltage references for the fast current regulation, which cannot be solved only by the overmodulation approaches.

On the other hand, there were different approaches to modifying the current trajectory for minimum transient time based on the optimal control theory [7], [8]. Using time optimal control (TOC), the voltage references for the optimal current trajectory can be mathematically derived depending on the saturated voltage condition after disengaging the voltage reference of the PI current controller. However, the online derivation of the voltage references is a computation burden to a digital signal processor.

Some algorithms modifying current references based on current error feedback [9], [10] were introduced. For the fast regulation of the q-axis current, the q-axis current error in the transient state is subtracted from the d-axis current reference. The experimental results show quite good current tracking performance under the base speed [9] and in the flux weakening region [10]. Although it achieves a fast transient response, the current error feedback method cannot be solely utilized as a flux weakening algorithm because steady-state errors in the d-/q-axis currents are unavoidable in the flux weakening region.

In this paper, a novel current control scheme for fast transient response is proposed. The basic concept is to alleviate the

Manuscript received May 26, 2011; revised August 1, 2011; accepted September 25, 2011. Date of publication December 5, 2011; date of current version April 13, 2012.

The authors are with Seoul National University, Seoul 151-742, Korea (e-mail: dydcjfe@eepel.snu.ac.kr; ksmin@eepel.snu.ac.kr; sulsk@plaza.snu.ac.kr).

Color versions of one or more of the figures in this paper are available online at http://ieeexplore.ieee.org.

Digital Object Identifier 10.1109/TIE.2011.2173097

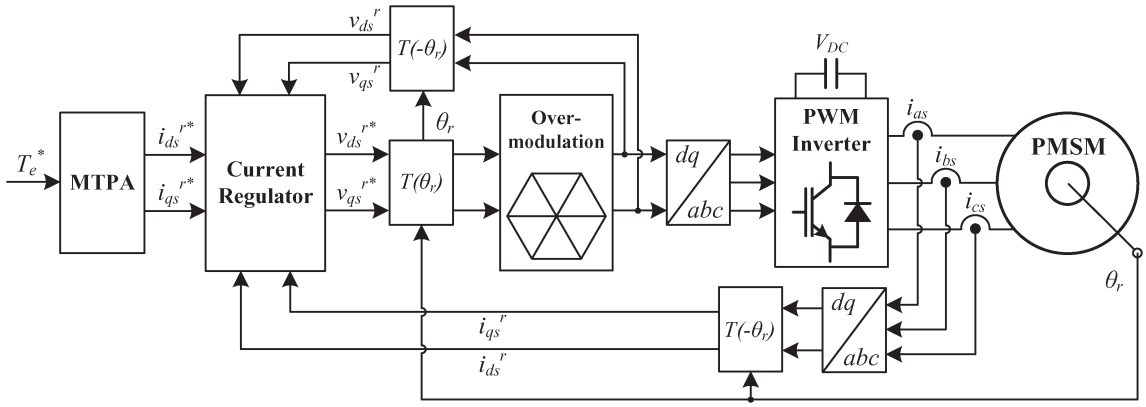

Fig. 1. Block diagram of the PMSM drive system using a synchronous frame PI current regulator.

voltage deficiency in the transient state by intensifying the d-axis current for a moment. Considering the voltage saturation, the references of the conventional PI regulator are modified to secure the voltage margin. The proposed method has different structures according to its applications, whether the flux weakening control is applied or not. Based on the analysis of the characteristics of the controller and the motor, the reference modification parts are well designed in both applications. Using the proposed method, the transient response is improved, which is indicated as the reduced settling time. In order to prove the effectiveness of the proposed scheme, the simulation and experimental results are presented.

II. Conventional Control Scheme [11]

The voltage and torque equations of a salient PMSM in a synchronous reference frame are expressed as

$$\begin{aligned} v_{ds}^r &= R_s i_{ds}^r + sL_d i_{ds}^r + e_{ds}^r \\ v_{qs}^r &= R_s i_{qs}^r + sL_q i_{qs}^r + e_{qs}^r \end{aligned} \tag{1}$$

$$\begin{aligned} e_{ds}^r &= -\omega_r L_q i_{qs}^r \\ e_{qs}^r &= \omega_r \left(L_d i_{ds}^r + \lambda_f\right) \end{aligned} \tag{2}$$

$$T_e = \frac{3}{2}\frac{P}{2}\left\{\lambda_f i_{qs}^r + (L_d - L_q) i_{ds}^r i_{qs}^r\right\} \tag{3}$$

where

superscript "r"	synchronous reference frame;
v_{ds}^r, v_{qs}^r	$d-q$ components of stator voltage;
e_{ds}^r, e_{qs}^r	$d-q$ components of effective back-EMF;
i_{ds}^r, i_{qs}^r	$d-q$ components of stator current;
R_s	stator resistance;
L_d, L_q	$d-q$ components of stator self-inductance;
ω_r	electrical speed;
λ_f	stator flux linkage of permanent magnet;
P	number of poles.

e_{ds}^r and e_{qs}^r are the effective back-EMF voltages including the d-/q-axis coupling voltage terms and back-EMF voltage due to the permanent magnet flux linkage, which are compensated by the feedforwarding control in the current regulation loop. In surface-mounted PMSMs (SMPMSMs), L_d and L_q are identical because of the machine's nonsalient structure. On the other hand, the interior PMSM (IPMSM) has different L_d and L_q because of its salient structure. In the conventional IPMSM design, L_q is larger than L_d.

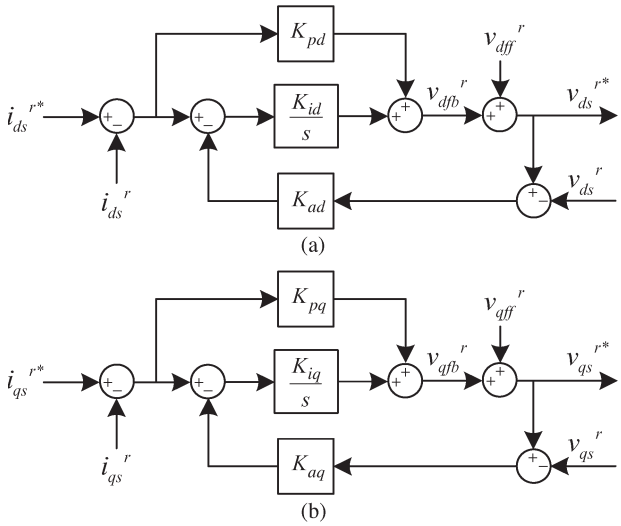

Fig. 2. Structure of synchronous current regulator with feedforward decoupling and anti-windup controls. (a) d- and (b) q-axis current controls.

The block diagram of the PMSM drive system using a synchronous frame current regulator is shown in Fig. 1. From the torque reference, the q-axis current reference is decided according to the torque-constant and/or maximum-torque-per-ampere operating condition. A detailed description of the current regulator is shown in Fig. 2. The classical anti-windup method using back calculation [12] is used to improve transient response. The feedback voltage terms are expressed as

$$\begin{aligned} v_{dfb}^r &= \frac{sK_{pd} + K_{id}}{s}\Delta i_{ds}^r - \frac{K_{ad}K_{id}}{s}\Delta v_{ds}^r \\ v_{qfb}^r &= \frac{sK_{pq} + K_{iq}}{s}\Delta i_{qs}^r - \frac{K_{aq}K_{iq}}{s}\Delta v_{qs}^r \end{aligned} \tag{4}$$

where Δi_{ds}^r, Δi_{qs}^r, Δv_{ds}^r, and Δv_{qs}^r are current errors and voltage differences defined as

$$\begin{aligned} \Delta i_{ds}^r &= i_{ds}^{r^*} - i_{ds}^r \\ \Delta i_{qs}^r &= i_{qs}^{r^*} - i_{qs}^r \\ \Delta v_{ds}^r &= v_{ds}^{r^*} - v_{ds}^r \\ \Delta v_{qs}^r &= v_{qs}^{r^*} - v_{qs}^r. \end{aligned} \tag{5}$$

TABLE I
GENERAL GAIN SETTINGS

K_{pd}	K_{id}	K_{ad}	K_{pq}	K_{iq}	K_{aq}
$L_d\omega_{cc}$	$R_s\omega_{cc}$	$\frac{1}{K_{pd}}$	$L_q\omega_{cc}$	$R_s\omega_{cc}$	$\frac{1}{K_{pq}}$

ω_{cc}: The bandwidth of the current regulator.

Effective back-EMFs, e^r_{ds} and e^r_{qs}, are compensated by decoupling control in feedforward manner. Feedforwarding terms are expressed as

$$\begin{aligned} v^r_{dff} &= -\omega_r \hat{L}_q i^r_{qs} \\ v^r_{qff} &= \omega_r \left(\hat{L}_q i^r_{qs} + \hat{\lambda}_f\right) \end{aligned} \tag{6}$$

where $\hat{L}_d$, $\hat{L}_q$, and $\hat{\lambda}_f$ indicate the estimated values of L_d, L_q, and λ_f, respectively. If the estimated values are identical to the real values, effective back-EMFs are completely compensated by feedforwarding terms. The outputs of the current regulator consist of feedback and feedforwarding voltage terms expressed as follows:

$$\begin{aligned} v^{r^*}_{ds} &= v^r_{dfb} + v^r_{dff} \\ v^{r^*}_{qs} &= v^r_{qfb} + v^r_{qff}. \end{aligned} \tag{7}$$

The general settings of the PI and anti-windup gains are listed in Table I. In the table, ω_{cc} stands for the bandwidth of the current regulator.

In the unsaturated condition, the voltage references can be exactly synthesized by an inverter. Ignoring the parameter error and signal processing delay, the transfer function of d-/q-axis current regulators can be expressed as follows:

$$\begin{aligned} i^r_{ds} &= \frac{\omega_{cc}}{s+\omega_{cc}} i^{r^*}_{ds} \\ i^r_{qs} &= \frac{\omega_{cc}}{s+\omega_{cc}} i^{r^*}_{qs}. \end{aligned} \tag{8}$$

The transfer functions of the closed-loop system are set as that of the first-order low-pass filter whose response is well defined without any overshoot and steady-state error. As seen from (8), the bandwidth of the regulator is ω_{cc} as designed.

In the saturated condition, the output voltage of the current regulator cannot be synthesized. Because of the limited dc-link voltage, a point on the hexagonal voltage boundary is selected as the synthesized output voltage according to a specific overmodulation method. Considering the voltage difference between the output voltage of current regulator and the synthesized voltage by the inverter, the transfer function of the d-/q-axis currents are derived as follows:

$$\begin{aligned} i^r_{ds} &= \frac{\omega_{cc}}{s+\omega_{cc}} \left(i^{r^*}_{ds} - \frac{\Delta v^r_{ds}}{L_d\omega_{cc}}\right) \\ i^r_{qs} &= \frac{\omega_{cc}}{s+\omega_{cc}} \left(i^{r^*}_{qs} - \frac{\Delta v^r_{qs}}{L_q\omega_{cc}}\right). \end{aligned} \tag{9}$$

In the saturated condition, the voltage difference terms appear in the transfer function as a disturbance input. These terms degrade the current regulation performance in the transient state.

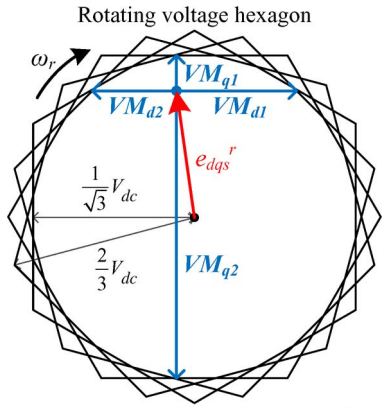

VM_{d1}: Voltage margin for increasing i^r_{ds}.
VM_{d2}: Voltage margin for decreasing i^r_{ds}.
VM_{q1}: Voltage margin for increasing i^r_{qs}.
VM_{q2}: Voltage margin for decreasing i^r_{qs}.

Fig. 3. Vector diagram in synchronous reference frame.

III. PROPOSED CURRENT CONTROL SCHEME

A. Consideration on Voltage Margin

Dynamic voltage is the voltage which invokes the actual variation of current. The dynamic voltage can be expressed in vector notation as

$$v^r_{dyn} = v^r_{dqs} - e^r_{dqs}. \tag{10}$$

From the voltage equations in (1), the dynamic voltages and its resultant responses are expressed as follows:

$$\begin{aligned} v^r_{ddyn} &= v^r_{ds} - e^r_{ds} \approx L_d \frac{di^r_{ds}}{dt} \\ v^r_{qdyn} &= v^r_{qs} - e^r_{qs} \approx L_q \frac{di^r_{qs}}{dt}. \end{aligned} \tag{11}$$

Equation (11) means that, for the fast current regulation, a large magnitude of the dynamic voltage is required. Fig. 3 shows the vector diagram describing the voltage margin in the synchronous reference frame. Because the voltage margin, defined in Fig. 3, determines the dynamic voltage, it is important to prepare the voltage margin in the transient state for faster current regulation. In medium to rated speed, e^r_{qs} becomes larger as the back-EMF voltage by the permanent magnet flux linkage λ_f grows in proportion to electrical speed. Because the voltage margin for increasing i^r_{qs}, denoted as VM_{q1}, is smaller at higher rotating speed, as shown in Fig. 3, the torque current cannot increase rapidly. On the other hand, the voltage margin for decreasing i^r_{qs}, denoted as VM_{q2}, is large enough, and the q-axis current can be decreased as the designed bandwidth. Compared with VM_{q1}, the d-axis voltage margins are relatively large.

B. Proposed Control Scheme Under the Base Speed

In order to improve the transient state, a novel control scheme based on the voltage feedback is proposed. As shown in Fig. 3, the q-axis voltage deficiency is much larger than the d-axis voltage deficiency in the PMSM. By concentrating on the alleviation of the q-axis voltage deficiency, the dynamic performance can be improved. One way of alleviating the q-axis voltage deficiency is to increase the voltage margin by reducing

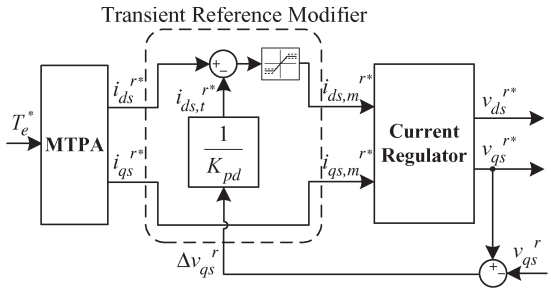

Fig. 4. Proposed control scheme under the base speed.

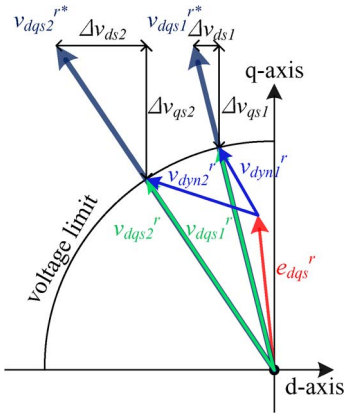

Fig. 5. Modification of voltage reference vector.

the magnitude of e_{qs}^r in proportion to the q-axis voltage difference, which stands for the q-axis voltage deficiency. In order to reduce e_{qs}^r, $i_{ds}^{r^*}$ is modified in the transient state.

The proposed control scheme is shown in Fig. 4. In the proposed method, the transient reference modifier is added before the current regulator. The modified d-axis current reference, denoted as $i_{ds,m}^{r^*}$, is expressed as

$$i_{ds,m}^{r^*} = i_{ds}^{r^*} - i_{ds,t}^{r^*} = i_{ds}^{r^*} - \frac{1}{K_{pd}} \Delta v_{qs}^r. \tag{12}$$

The feedback gain $1/K_{pd}$ is designed in a way that Δv_{qs}^r is subtracted instantaneously from the d-axis voltage reference. If the modified reference in (12) passes through the d-axis PI controller, its resultant d-axis voltage reference is approximated as (13) under the assumption that $K_{id} = R_s \omega_{cc}$ is much smaller than the magnitude of sK_{pd}. That assumption can be justified because the transient reference modifier usually operates for a short time

$$v_{ds2}^{r^*} = v_{ds1}^{r^*} - \frac{sK_{pd} + K_{id}}{s} \frac{\Delta v_{qs2}^r}{K_{pd}} \approx v_{ds1} r^* - \Delta v_{qs2}^r \tag{13}$$

where $v_{ds2}^{r^*}$ and Δv_{qs2} are the values with voltage feedback control and $v_{ds1}^{r^*}$ and Δv_{qs1} are the values without voltage feedback control.

Fig. 5 shows the effect of the modification of the voltage reference in (13) when a step torque command is applied. In this figure, the hexagonal voltage boundary is approximated as a circle for simplicity. When a step torque command is applied, q-axis voltage reference is rapidly pushed outside the voltage limit. Applying voltage feedback control, the voltage reference is shifted to the left side, which is expressed in (13), and the

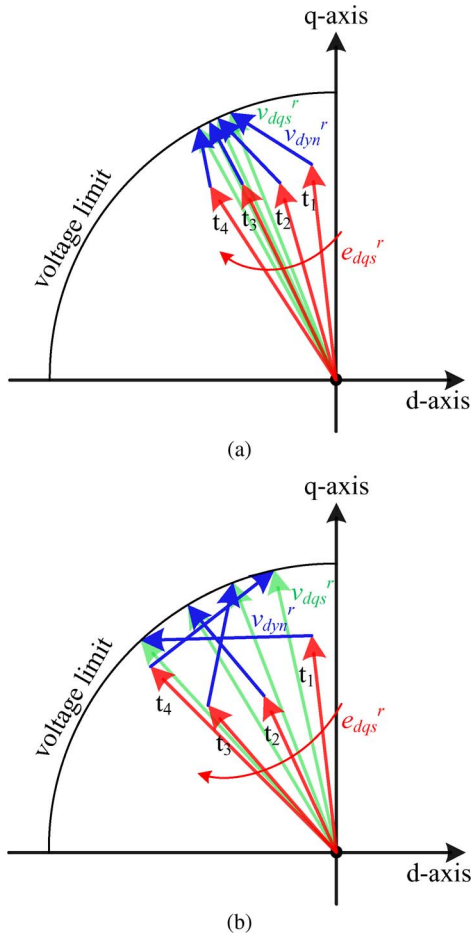

Fig. 6. Transition of effective back-EMF and dynamic voltage using the (a) conventional and (b) proposed controls.

voltage assigned by dynamic overmodulation is changed from v_{dqs1}^r to v_{dqs2}^r. Finally, the dynamic voltage is also changed from v_{dyn1}^r to v_{dyn2}^r. This modified dynamic voltage pushes the d-axis current toward the negative direction, correcting current trajectory.

In order to regulate the magnitude of the current within a maximum value, the modified current reference is limited as (14) by a limiter in Fig. 4

$$-\sqrt{I_{s,\max}^2 - i_{qs}^{r2}} \le i_{ds,m}^{r^*} \le \sqrt{I_{s,\max}^2 - i_{qs}^{r2}} \tag{14}$$

where $I_{s,\max}$ is the maximum allowable peak current in the transient state. Using the limiter, the magnitude of the currents are guaranteed to be lower than $I_{s,\max}$.

In the voltage unsaturated condition, the transient response is the same as the original response in (8). In the saturated condition, the responses are expressed as

$$\begin{aligned} i_{ds}^r &= \frac{\omega_{cc}}{s+\omega_{cc}} \left\{ i_{ds}^{r^*} - \frac{1}{L_d \omega_{cc}} \left(\Delta v_{ds}^r + \Delta v_{qs}^r \right) \right\} \\ i_{qs}^r &= \frac{\omega_{cc}}{s+\omega_{cc}} \left(i_{qs}^{r^*} - \frac{1}{L_q \omega_{cc}} \Delta v_{qs}^r \right). \end{aligned} \tag{15}$$

Compared with the responses in (9), a q-axis voltage difference related term is added in the d-axis current. This term modifies the d-axis current in the transient state, securing the q-axis voltage margin.

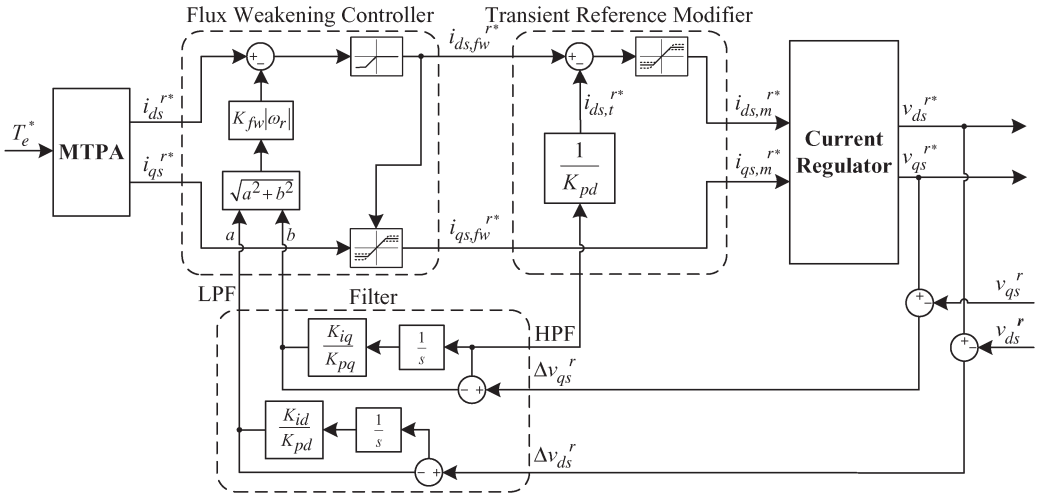

Fig. 7. Proposed flux weakening scheme.

In Fig. 6, a symbolic diagram is shown for an easy understanding of the transition of the effective back-EMF vector from the observation of simulation results. With respect to the time passing, the effective back-EMFs expressed as (2) and the dynamic voltages are drawn. At t_1, a step torque command is applied. As shown in Fig. 6(a), e^r_{dqs} directly moves toward the final point slowly because of the q-axis voltage deficiency. Using the proposed method, however, e^r_{qs} is reduced because i^r_{ds} is reduced toward the negative direction by the voltage feedback control. This procedure helps to secure VM_{q1} in the transient state, as shown in Fig. 6(b). Moreover, the current regulation in Fig. 6(b) is faster than that in Fig. 6(a), which is also verified by the computer simulations and experimental results in the next chapter.

C. Proposed Control Scheme in the Flux Weakening Region

With a simple modification of the controller, the proposed method can also be applied for improving the transient performance of the flux weakening control. Among many flux weakening methods [13]–[21], many parameter-insensitive flux weakening methods [17]–[21] utilize the feedback signals to determine the steady-state current references. For higher torque generation in the steady state, an algorithm based on low-pass-filtered voltage difference signals [20], [21] is a proper choice. Because the voltage reference rotates in the overmodulation region, a high modulation index is obtained, which leads to high torque production.

At the steady state within the flux weakening condition, the dc value of the voltage difference is kept as a constant. Then, the dc components of Δv^r_{ds} and Δv^r_{qs} in (15) influence the steady-state d-/q-axis currents, causing a steady-state error [20], [21]. Thus, in the flux weakening region, the anti-windup controller based on the back calculation method is intentionally taken out of the control loop. Then, the transient response of the conventional PI regulator is derived as

$$i^r_{ds} = \frac{\omega_{cc}}{s+\omega_{cc}} i^{r^*}_{ds} - \frac{s}{(s+\omega_{cc})(sL_d+R_s)}\Delta v^r_{ds}$$
$$i^r_{qs} = \frac{\omega_{cc}}{s+\omega_{cc}} i^{r^*}_{qs} - \frac{s}{(s+\omega_{cc})(sL_q+R_s)}\Delta v^r_{qs}. \quad (16)$$

In (16), the dc components of Δv^r_{ds} and Δv^r_{qs} diminish in the steady state. Thus, the operating currents are decided by the flux weakening controller.

Fig. 7 shows the proposed flux weakening scheme. The proposed method consists of two parts: flux weakening controller and transient reference modifier. The algorithm based on low-pass-filtered voltage difference signals [20], [21] is adopted as the flux weakening controller. A filter is implemented by using a simple feed-back loop to produce signals used in the flux weakening controller and the transient reference modifier. The d-axis flux weakening reference is expressed as

$$i^{r^*}_{ds,fw} = i^{r^*}_{ds} - K_{fw}|\omega_r|\sqrt{LPF_d^2 + LPF_q^2}$$
$$LPF_d = \frac{K_{id}}{sK_{pd}+K_{id}}\Delta v^r_{ds}$$
$$LPF_q = \frac{K_{iq}}{sK_{pq}+K_{iq}}\Delta v^r_{qs}. \quad (17)$$

Because $i^{r^*}_{ds,fw}$ is calculated from the low-pass-filtered signal, the dc components of Δv_{dsr} and Δv_{qsr} determine the steady-state current references. The flux weakening current references, namely, $i^{r^*}_{ds,fw}$ and $i^{r^*}_{qs,fw}$, are limited by

$$-I_{s,\text{rated}} \le i^{r^*}_{ds,fw} \le 0$$
$$-\sqrt{I^2_{s,\text{rated}} - i^{r^*}_{ds,fw}} \le i^{r^*}_{qs,fw} \le \sqrt{I^2_{s,rated} - i^{r^*}_{ds,fw}} \quad (18)$$

where $I_{s,\text{rated}}$ is the peak value of the rated current.

In the flux weakening controller [20], [21], K_{fw} is an important gain which enforces a tradeoff between the transient current control performance and the torque capacity. Although decreasing K_{fw} makes the output torque higher, the control performance is degraded by that. Thus, in achieving a higher torque capability, which is realized by setting a low value for K_{fw}, the degradation of the control performance is unavoidable in the conventional method [20], [21].

The proposed method is characterized by the utilization of an additional high-frequency signal, which is shown in Fig. 7. The transient reference modifier utilizes the high-pass-filtered

TABLE II
PARAMETERS OF IPMSM UNDER TEST

Rated Power	11kW
Rated voltage	$190V_{rms}$
Rated current	$38A_{rms}$
Number of poles	6 poles
R_s	0.15 Ω
λ_f	$0.254V_{peak}/(rad/s)$
L_d	3.6mH
L_q	4.3mH

signal for modifying the d-axis current reference in transient state. In Fig. 7, $i^{r^*}_{ds,t}$ is expressed as

$$i^{r^*}_{ds,t} = \frac{K_{pq}}{K_{pd}} \frac{s}{sK_{pq} + K_{iq}} \Delta v^r_{qs}. \tag{19}$$

This term modifies the current references in the transient state, and the transient responses of the currents are improved even with low value of K_{fw}. Finally, owing to this high-frequency signal, both higher torque capability and better control performance can be achieved, as verified in the simulations and experiments. The modified current references, $i^{r^*}_{ds,m}$ and $i^{r^*}_{qs,m}$, are also limited in the same range detailed in (14). Using the proposed method, the transfer function of d-/q-axis current regulators are deduced as

$$\begin{aligned} i^r_{ds} &= \frac{\omega_{cc}}{s+\omega_{cc}} i^{r^*}_{ds,fw} - \frac{s}{(s+\omega_{cc})(sL_d + R_s)} \Delta v^r_{ds} \\ &\quad - \rho \frac{s}{(s+\omega_{cc})(sL_q + R_s)} \Delta v^r_{qs} \\ i^r_{qs} &= \frac{\omega_{cc}}{s+\omega_{cc}} i^{r^*}_{qs,fw} - \frac{s}{(s+\omega_{cc})(sL_q + R_s)} \Delta v^r_{qs} \end{aligned} \tag{20}$$

where ρ is the saliency ratio defined as L_q/L_d. The third term in i^r_{ds} works as a preparation for the q-axis voltage margin in transient state.

IV. SIMULATION RESULTS

In order to verify the performance of the proposed method, computer simulations are carried out with Matlab Simulink. In the simulation, a 11-kW IPMSM is used, and its parameters are listed in Table II. The sampling period and switching frequency are set as 0.1 ms and 5 kHz, respectively. The bandwidth of the current control loop is 300 Hz, and the dc link voltage is limited as 280 V.

First, the proposed current control scheme without the flux weakening algorithm is simulated. Fig. 8 shows the d-/q-axis currents in the time domain from the simulation results using the algorithm described in Fig. 4. In this simulation, the speed is maintained at 1300 r/min by the load machine. At $t = 1$ ms, an abrupt torque command change from zero to maximum torque is applied. $I_{s,\max}$ in (3) is set as two times the rated peak current because $I_{s,max}$ is an instant maximum value of the current. The waveforms in Fig. 8(a) show the result from the conventional method, with 8.4-ms settling time. Because of the voltage deficiency, the current tracking performance is degraded. Fig. 8(b) shows the result from the proposed method, with 3.5-ms settling time. Due to the modified d-axis reference

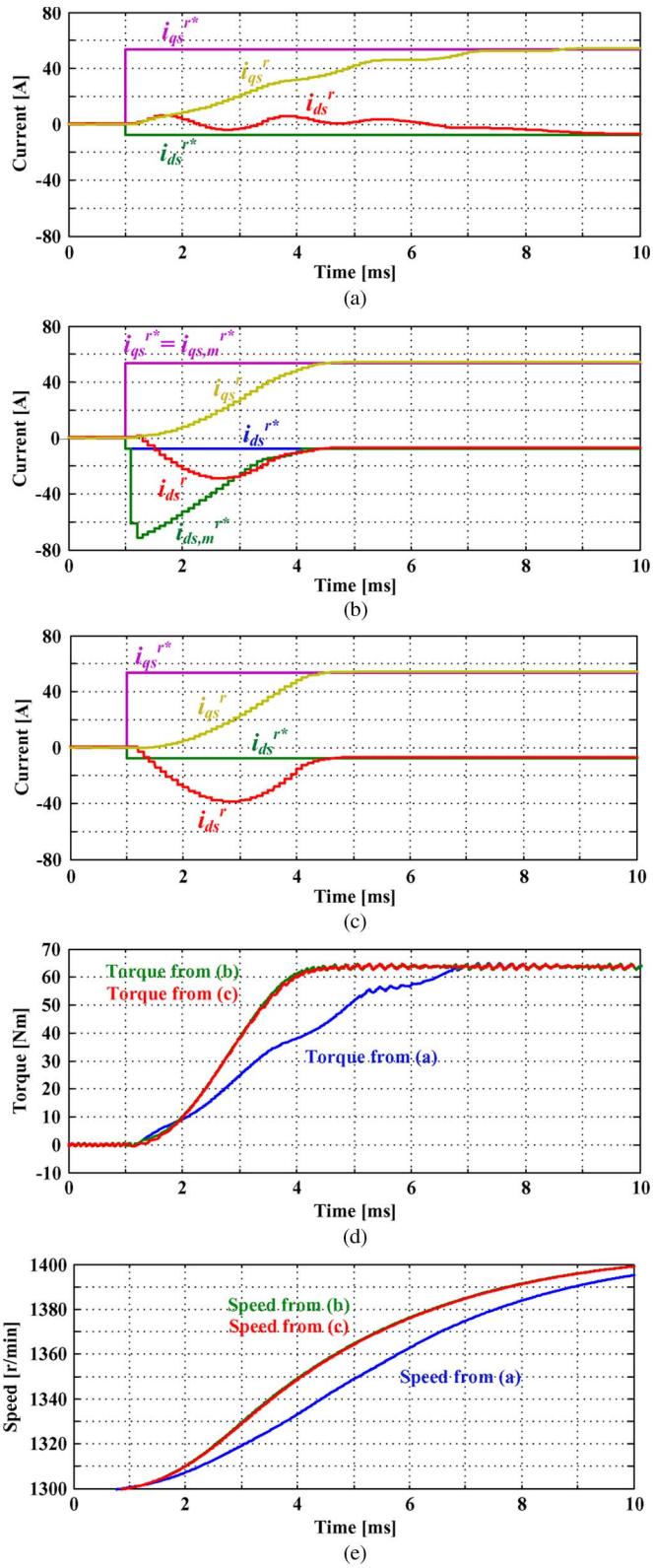

Fig. 8. Simulation results at middle speed. Current waveforms from (a) the conventional method, (b) the proposed method, and (c) the time optimal solution. (d) Torque behaviors from (a)–(c). (e) Speed behaviors from (a)–(c).

$i^r_{ds,m}$, the actual d-axis current is reduced to negative in the transient state. Because of that, the q-axis voltage margin is increased and the q-axis current regulation performance in the transient state is significantly improved. Fig. 8(c) shows the

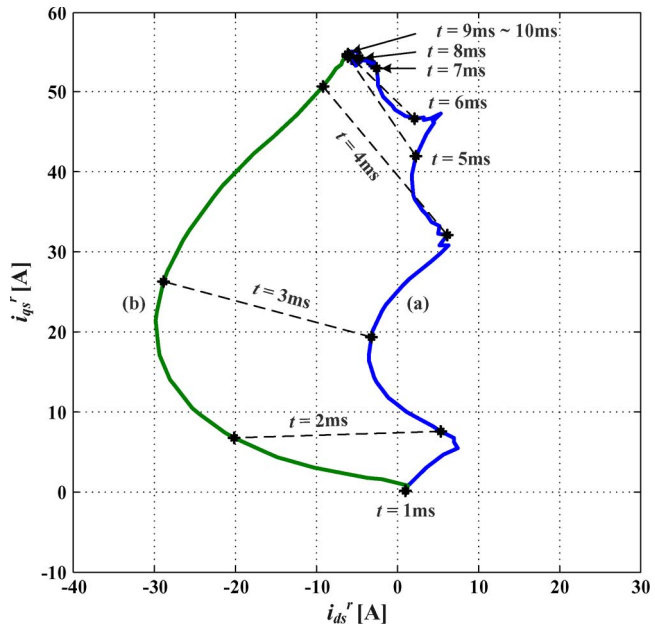

Fig. 9. Trajectories of $d-q$ currents from (a) the conventional method and (b) the proposed method.

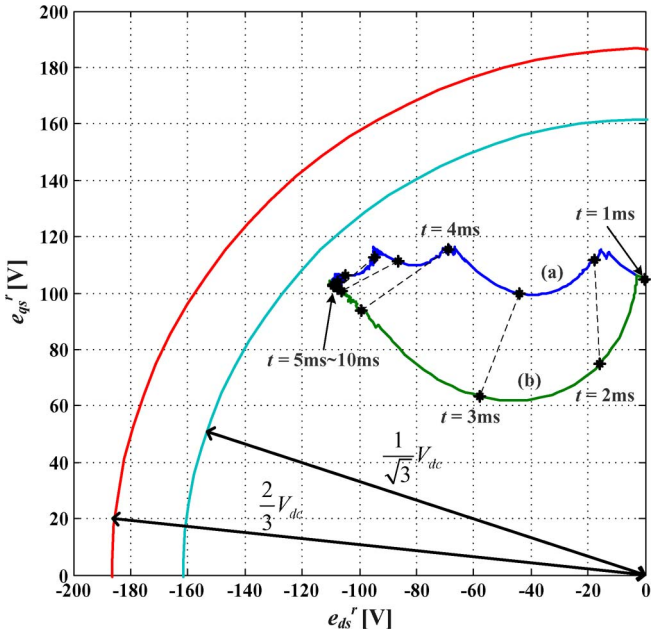

Fig. 10. Trajectories of effective back-EMFs from (a) the conventional method and (b) the proposed method.

result of the current regulation by the time optimal solution. As derived in [7] and [8], the voltage set by the time optimal solution voltage for the fastest transient response is a fixed point on the voltage hexagon in stationary reference frame. Therefore, the time optimal solution can be deduced by applying several points on the voltage hexagon in a trial-and-error manner without the complicated implementation of iteration procedure required in [7] and [8] for easy comparison. As shown in Fig. 8(b) and (c), the settling times of both cases are almost the same. With a simple modification of the current reference by the proposed method, the dynamic performance can be at par with that by the TOC. The traces of the torque with control methods in Fig. 8(a)–(c) are shown in Fig. 8(d). From the figure, the proposed method reveals significantly better torque response, which is similar to the torque response by the time optimal solution, compared with the response by the conventional method. In Fig. 8(e), the speed behaviors with control methods in Fig. 8(a)–(c) are also shown.

In Figs. 9 and 10, the trajectories of the d-/q-axis currents and effective back-EMFs are shown, respectively. The effective back-EMFs can be extracted from the PMSM model in the simulation. As shown in Fig. 9, the current trajectory is modified into a shortcut trajectory which exploits more d-axis current in the negative direction. Because of that, as shown in Fig. 10, the q-axis effective back-EMF is reduced in the transient state. In Fig. 10, the area between the trajectories (a) and (b) indicates an additional voltage margin which is obtained by the proposed method. Owing to this margin, the proposed method presents a significantly improved dynamic performance in the current regulation.

Second, the proposed current control scheme with the flux weakening control is simulated. As a flux weakening algorithm, the low-pass-filtered voltage difference feedback algorithm [20], [21] is employed. In the flux weakening region, the "conventional method" indicates the flux weakening method without the transient reference modifier. Fig. 11 shows the current control performance with the proposed method in the flux weakening condition. In this simulation, the flux weakening gain K_{fw} is set as a low value, i.e., 100 μ[As/V], for a purpose of high torque capacity. The mechanical speed of the test machine is maintained at 1800 r/min by the load machine. A maximum torque command is applied at $t = 0.1$ s. Moreover, at $t = 0.8$ s, the torque command is turned back to zero. In Fig. 11(a), the transient current control performance is apparently poor because of the low K_{fw}. More than 0.2 s is taken for the settlement of the currents, and overshoot and undershoot are observed in the current waveform. In Fig. 11(b), the transient current control performance is improved by applying the voltage feedback control even with the same K_{fw} in Fig. 11(a).

For a more reasonable evaluation of the current control performance in the flux weakening region, a performance index is defined as (21), which is the average rms current error during the regulation of the current for a fixed time interval

$$I_{\text{rms\_error}} = \sqrt{\frac{\int_{t_0}^{t_f}\left\{\left(i_{ds,fw}^{r*} - i_{ds}^{r}\right)^2 + \left(i_{qs,fw}^{r*} - i_{qs}^{r}\right)^2\right\}dt}{t_f - t_0}} \tag{21}$$

where t_0 and t_f are set to 0 and 1 s, respectively. Equation (21) is the calculation of standardized distance between the current reference and real current. Thus, $I_{\text{rms\_error}}$ becomes smaller with higher dynamics and more accurate controller. Fig. 11 shows $I_{\text{rms\_error}}$ contours calculated in various operating conditions. The Y-axis indicates the applied torque command, and the x-axis indicates the operating speed. Both axis values are written in per unit values. As described in Fig. 12, as torque command increases and operating speed becomes higher, the current tracking performance represented by $I_{\text{rms\_error}}$ is degraded. However, the degradation can be remarkably reduced by the proposed method.

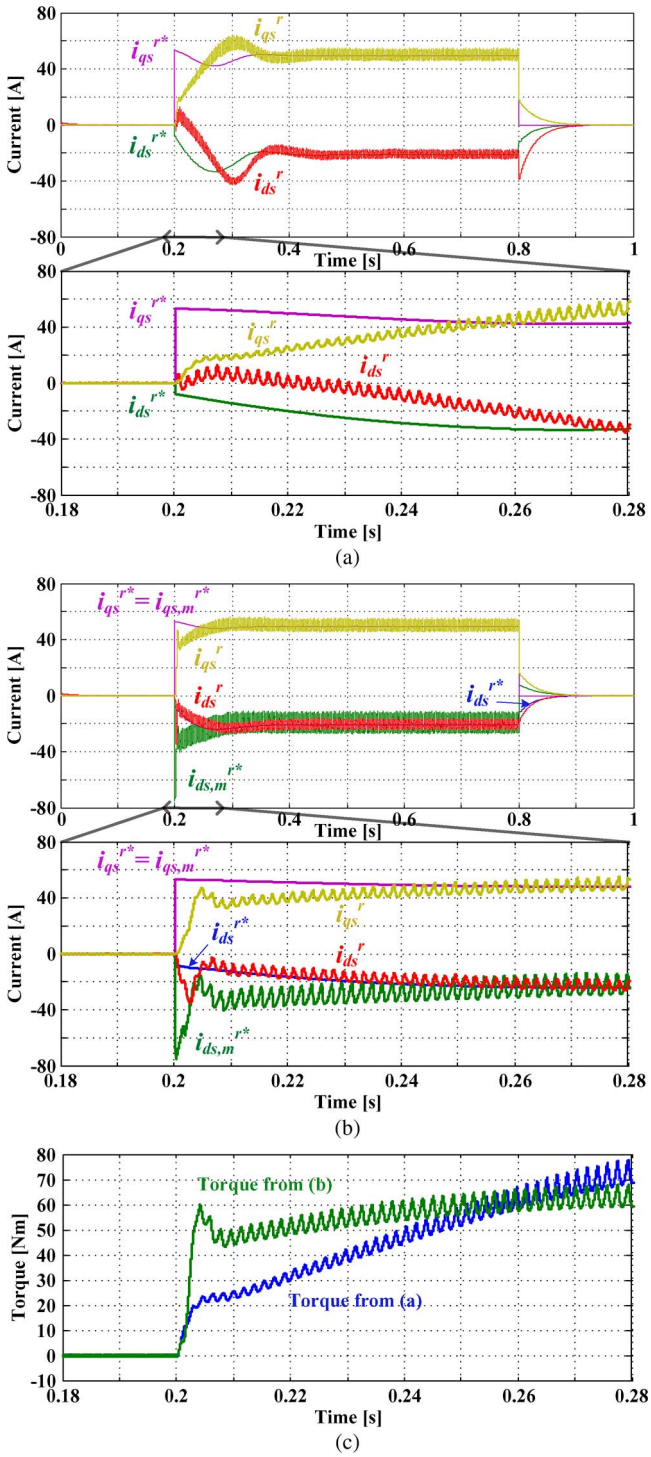

Fig. 11. Simulation results in the flux weakening region using (a) the conventional method and (b) the proposed method. (c) Torque behaviors from (a) and (b).

V. Experimental Results

Fig. 13 shows the experimental motor–generator set. An 11-kW IPMSM was used as a target machine, and the load machine is controlled so as to simulate the load conditions. The machine parameters are identical with those in the simulations. In Fig. 14, the experimental results under the same test conditions are shown with the simulation results in Fig. 8. From the figure, it is seen that the proposed strategy achieves a remarkably improved dynamic performance. The results show

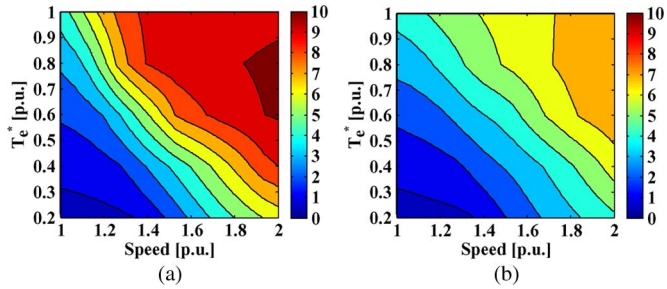

Fig. 12. Performance index contours from (a) the conventional and (b) proposed methods.

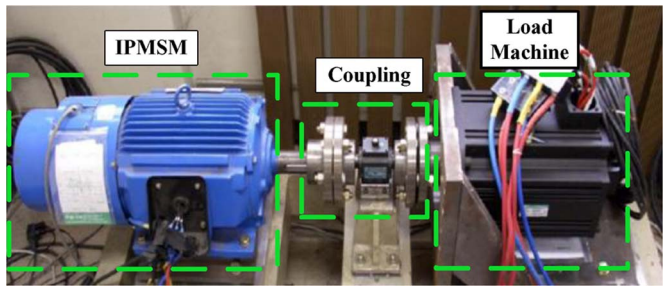

Fig. 13. Experimental setup.

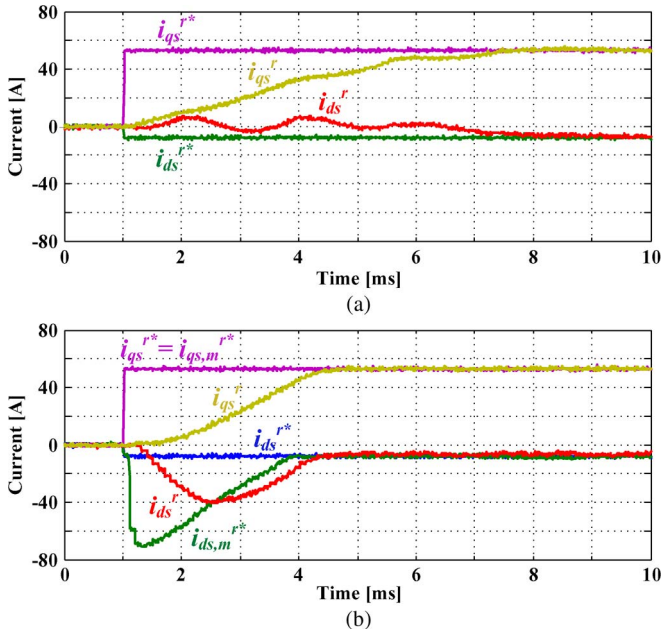

Fig. 14. Experimental results at middle speed using (a) the conventional and (b) proposed methods.

that the settling time of the proposed method is reduced by 55% compared with that of the conventional one in the case of d-axis current regulation.

In Fig. 15, a free acceleration test result is shown to demonstrate higher torque capability under the same voltage and current limitations. At 1300 r/min in a steady state, a maximum torque command is applied for 8 ms with no external load torque. As shown in Fig. 15(c), the acceleration rate of the proposed method is larger than that of the conventional method. At 9 ms, ω_{rpm2} has reached to 1429 r/min, whereas ω_{rpm1} has reached to 1414 r/min. Usually, the speed is determined by the time integral of the applied torque. Therefore, it can be noted

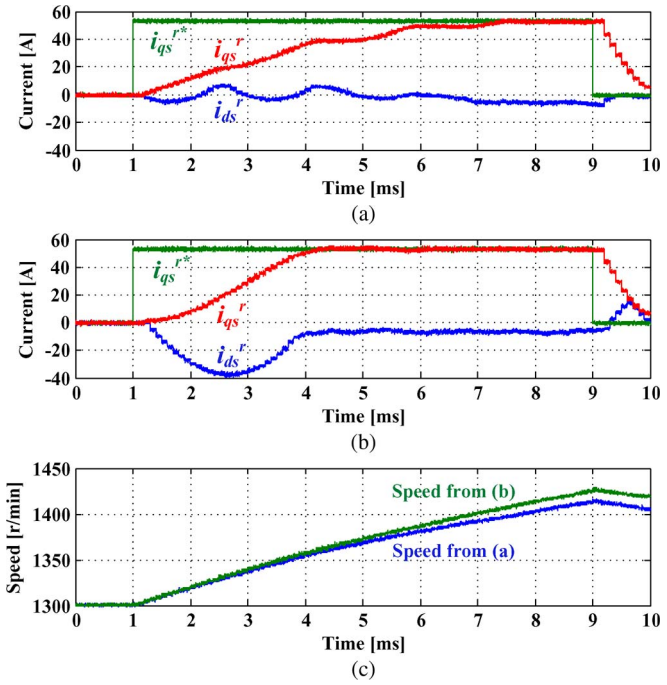

Fig. 15. Experimental results from free acceleration tests. (a), (b) $d-q$ currents from the conventional and proposed methods, respectively. (c) Speed behaviors from (a) and (b).

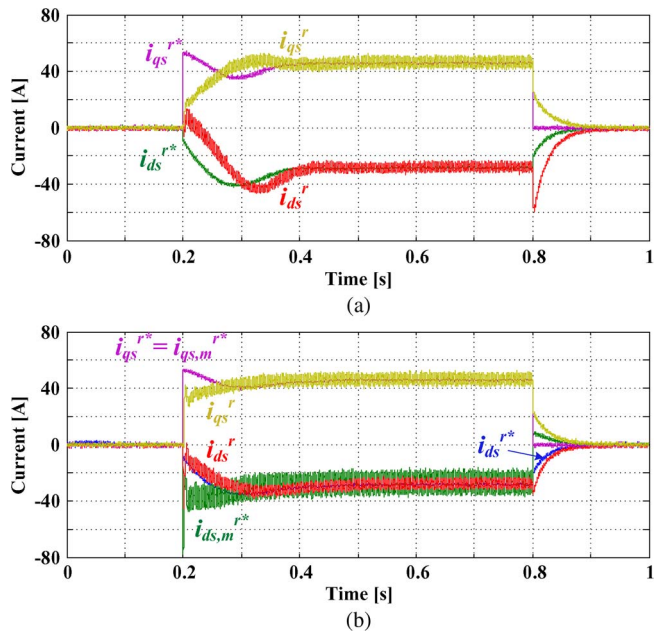

Fig. 16. Experimental results in flux weakening region using (a) the conventional and (b) proposed methods.

that higher torque has been generated by the proposed method in the transient state.

Fig. 16 shows the flux weakening experimental results under the same test conditions of the simulation results in Fig. 11. From the figure, it is seen that the capability of the drive system is enhanced in the transient condition by the voltage feedback current control scheme. The performance index $I_{\mathrm{rms\_error}}$ for the conventional method is 10.76 A, and that for the proposed method is 6.38 A, which is 40.7% lower than that for the conventional one.

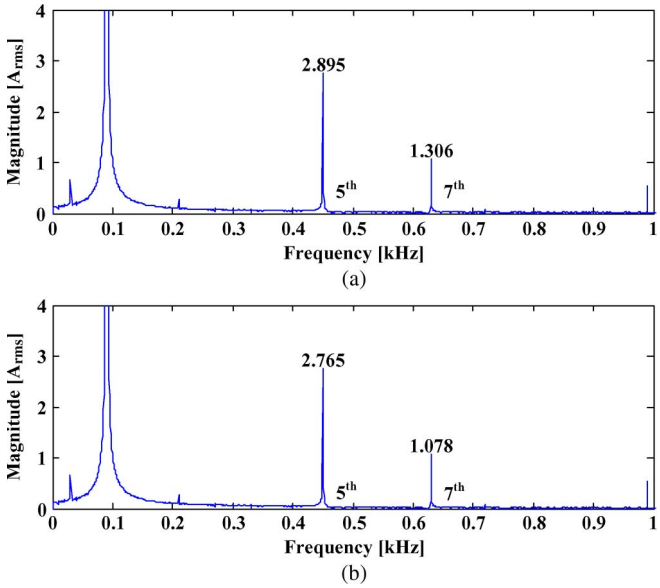

Fig. 17. Harmonic spectra of i_{as} from (a) the conventional and (b) proposed methods.

In Figs. 11 and 16, the sixth harmonic ripples are observed in the current waveforms. These sixth harmonics are, by nature, of the employed flux weakening algorithm [20], [21]. For high torque production, the overmodulation region is utilized by the flux weakening method. Because of this, the synthesized voltage contains sixth harmonics, and in turn, the actual current also contains sixth harmonics. The harmonic components in $i^{r^*}_{ds,m}$ are from the sixth harmonics in the synthesized q-axis voltage, v^r_{qs}. In the overmodulation region, the current regulation cannot be explained by the bandwidth of the current control loop itself. Because the synthesized voltage by the inverter is smaller than the voltage reference, the effective bandwidth of the current regulation is much lower than the designed bandwidth, i.e., 300 Hz. Because of this, the control system is not severely excited by the sixth harmonic components in $i^{r^*}_{ds,m}$. To verify this, the harmonic spectra of phase current calculated by fast Fourier transform is shown in Fig. 17. The operating condition is identical to that in Fig. 16. Upon comparing the harmonic components in (a) and (b), no significant difference in the steady-state current harmonics exists. Thus, it can be concluded that the steady-state characteristics are not deteriorated by the proposed method.

VI. Conclusion

In this paper, a novel control scheme for the fast current regulation has been proposed. In the medium to rated speed region, the current tracking is degraded due to the voltage deficiency coming from the high effective back-EMF voltage. In order to secure the voltage margin for current transition, the transient reference modifying algorithm has been devised. Using this algorithm, the d-axis current is reduced in transient state, securing the voltage margin. As a result, the dynamic performance is conspicuously improved without degrading the steady-state characteristics. The effectiveness of the proposed scheme is verified through computer simulations and experiments. The settling

time is reduced by 55%, and the average rms current error during the regulation has been reduced by 40.7% in the experiments.

REFERENCES

[1] T. M. Rowan and R. J. Kerkman, "A new synchronous current regulator and an analysis of current-regulated PWM inverters," *IEEE Trans. Ind. Appl.*, vol. IA-22, no. 4, pp. 678–690, Jul./Aug. 1986.

[2] A. M. Hava, S.-K. Sul, R. J. Kerkman, and T. A. Lipo, "Dynamic overmodulation characteristics of triangle intersection PWM methods," *IEEE Trans. Ind. Appl.*, vol. 35, no. 4, pp. 896–907, Jul./Aug. 1999.

[3] J. K. Seok, J.-S. Kim, and S. K. Sul, "Overmodulation strategy for high performance torque control," *IEEE Trans. Power Electron.*, vol. 13, no. 4, pp. 786–792, Jul. 1998.

[4] B. H. Bae and S. K. Sul, "A novel dynamic overmodulation strategy for fast torque control of high-saliency-ratio AC motor," *IEEE Trans. Ind. Appl.*, vol. 41, no. 4, pp. 1013–1019, Jul./Aug. 2005.

[5] S. Lerdudomsak, M. Kadota, S. Doki, and S. Okuma, "Novel techniques for fast torque response of IPMSM based on space-vector control method in voltage saturation region," in *Proc. IEEE IECON*, Nov. 2007, pp. 1015–1020.

[6] S. Lerdudomsak, S. Doki, and S. Okuma, "Voltage limiter calculation method for fast torque response of IPMSM in overmodulation range," in *Proc. IEEE IECON*, Nov. 2009, pp. 1383–1388.

[7] J. W. Choi and S. K. Sul, "Generalized solution of minimum time control in three-phase balanced systems," *IEEE Trans. Ind. Electron.*, vol. 45, no. 5, pp. 738–744, Oct. 1998.

[8] S. Bolognani, M. Tomasini, L. Tubiana, and M. Zigliotto, "DSP-based time optimal current control for high dynamic IPM motor drives," in *Proc. 35th Annu. IEEE PESC*, Jun. 20–25, 2004, vol. 3, pp. 2197–2203.

[9] J. W. Choi and S. K. Sul, "Design of fast-response current controller using d-q axis cross coupling application to permanent magnet synchronous motor drive," *IEEE Trans. Ind. Electron.*, vol. 45, no. 3, pp. 522–524, Jun. 1998.

[10] D. S. Maric, S. Hiti, C. C. Stancu, J. M. Nagashima, and D. B. Rutledge, "Two flux weakening schemes for surface-mounted permanent-magnet synchronous drives. Design and transient response considerations," in *Proc. ISIE*, 1999, pp. 673–678.

[11] S. K. Sul, *Control of Electric Machine Drive Systems*. New York: Wiley, 2011.

[12] C. Bohn and D. P. Atherton, "An analysis package comparing PID antiwindup strategies," *IEEE Control Syst. Mag.*, vol. 15, no. 2, pp. 34–40, Apr. 1995.

[13] S. Morimoto, Y. Takeda, T. Hirasa, and K. Taniguchi, "Expansion of operating limits for permanent magnet motor by current vector control considering inverter capacity," *IEEE Trans. Ind. Appl.*, vol. 26, no. 5, pp. 866–871, Sep./Oct. 1990.

[14] W. L. Soong and T. J. E. Miller, "Field-weakening performance of five classes of brushless synchronous AC motor drives," *Proc. Inst. Elect. Eng.—Elect. Power Appl.*, vol. 141, pt. B, no. 6, pp. 331–340, Nov. 1994.

[15] M. Tursini, E. Chiricozzi, and R. Petrella, "Feedforward flux-weakening control of surface-mounted permanent-magnet synchronous motors accounting for resistive voltage drop," *IEEE Trans. Ind. Electron.*, vol. 57, no. 1, pp. 440–448, Jan. 2010.

[16] B. Cheng and T. R. Tesch, "Torque feedforward control technique for permanent-magnet synchronous motors," *IEEE Trans. Ind. Electron.*, vol. 57, no. 3, pp. 969–974, Mar. 2010.

[17] J. Wai and T. M. Jahns, "A new control technique for achieving wide constant power speed operation with an interior PM alternator machine," in *Conf. Rec. IEEE IAS Annu. Meeting*, 2001, vol. 2, pp. 807–814.

[18] J. M. Kim and S. K. Sul, "Speed control of interior permanent magnet Synchronous motor drive for the flux weakening operation," *IEEE Trans. Ind. Appl.*, vol. 33, no. 1, pp. 43–48, Jan./Feb. 1997.

[19] S. M. Sue and C. T. Pan, "Voltage-constraint-tracking-based field-weakening control of IPM synchronous motor drives," *IEEE Trans. Ind. Electron.*, vol. 55, no. 1, pp. 340–347, Jan. 2008.

[20] T. S. Kwon and S. K. Sul, "Novel antiwindup of a current regulator of a surface-mounted permanent-magnet motor for flux-weakening control," *IEEE Trans. Ind. Appl.*, vol. 42, no. 5, pp. 1293–1300, Sep./Oct. 2006.

[21] T. S. Kwon, K. Y. Choi, M. S. Kwak, and S. K. Sul, "Novel flux-weakening control of an IPMSM for quasi-six-step operation," *IEEE Trans. Ind. Appl.*, vol. 44, no. 6, pp. 1722–1731, Nov./Dec. 2008.

Yong-Cheol Kwon (S'11) was born in Seoul, Korea, in 1986. He received the B.S. degree in electrical engineering from Seoul National University, Seoul, in 2010, where he is currently working toward the M.S. degree.

His current research interests include power electronics, electric machines, and sensorless drives.

Sungmin Kim (S'09) was born in Seoul, Korea in 1980. He received the B.S. and M.S. degrees in electrical engineering from Seoul National University, Seoul, in 2002 and 2008, respectively, where he is currently working toward the Ph.D. degree.

His current research interests are power electronics, machine design and drives, sensorless drives, and power conversion circuits.

Seung-Ki Sul (S'78–M'80–SM'98–F'00) was born in Korea in 1958. He received the B.S., M.S., and Ph.D. degrees in electrical engineering from Seoul National University, Seoul, Korea, in 1980, 1983, and 1986, respectively.

From 1986 to 1988, he was an Associate Researcher with the Department of Electrical and Computer Engineering, University of Wisconsin, Madison. From 1988 to 1990, he was a Principal Research Engineer with Gold-Star Industrial Systems Company. Since 1991, he has been a member of the faculty of the School of Electrical Engineering, Seoul National University, where he is currently a Professor and, from 2005 to 2007, was the Vice Dean of Electrical Engineering. Since 2008, he has been the President of Korea Electrical Engineering and Science Research Institute, Seoul. His current research interests are power-electronic control of electric machines, electric/hybrid vehicle drives, and power-converter circuits.